Environmental Stress Cracking of High-Density Polyethylene under plane stress conditions

Marco Contino*, Luca Andena, Marta Rink
Dipartimento di Chimica, Materiali e Ingegneria Chimica "G.Natta", Politecnico di Milano, Piazza Leonardo da Vinci 32, 20133 Milano, Italy

*Corresponding author. Tel.: +390223993146;
  E-mail address: marco.contino@polimi.it

Abstract

High-Density Polyethylene is prone to Environmental Stress Cracking if mechanically stressed in the presence of solutions containing surfactants. Even if this polymer is widely used to produce containers for industrial and household detergents, its Environmental Stress Cracking Resistance is generally evaluated under plane strain conditions irrespective of the actual stress state experienced during service life. In this work the Slow Crack Growth of thin specimens, under plane stress conditions, was studied in air and in the presence of an "active" environment. The J-integral approach was adopted to account for the extensive plastic deformations thereby occurring and the obtained results were compared to those describing the plane strain behaviour of the same polyethylene, reported in previous works. The effect of the production process was also assessed by comparing the behaviour of compression moulded and blow moulded specimens, the latter having a lower degree of crystallinity. Despite the difference in fracture resistance expected in air, the behaviour in presence of the active environment was very similar, suggesting that the production process has only negligible influence on the Environmental Stress Cracking resistance of the considered polyethylene.

Keywords

ESC, Slow crack growth, HDPE, plane stress, J-integral

Nomenclature

a	Notch length
a_i	Notch length of a generic blunt notched specimen used for the evaluation of the separation parameter
a_j	Notch length of the reference blunt notched specimen used for the evaluation of the separation parameter
t	Time
t_i	Initiation time
$t_{DB,pl.strain}$	Time at the ductile to brittle transition in plane strain
t_i^*	Critical interaction time
$t_{i,pl.strain}^*$	Critical interaction time in plane strain
$t_{i,pl.stress}^*$	Critical interaction time in plane stress
u	Displacement
u_i	Displacement at fracture initiation
$u_{i,BM}$	Displacement at fracture initiation for blow moulded specimens
$u_{i,CM}$	Displacement at fracture initiation for compression moulded specimens
u_{el}	Elastic displacement
$u_{el\,i,BM}$	Elastic displacement at fracture initiation for blow moulded specimens
$u_{el\,i,CM}$	Elastic displacement at fracture initiation for compression moulded specimens
u_{pl}	Plastic displacement
$u_{pl\,i,BM}$	Plastic displacement at fracture initiation for blow moulded specimens
$u_{pl\,i,CM}$	Plastic displacement at fracture initiation for compression moulded specimens
A	Generic constant
A_1	Generic constant
A_2	Generic constant
B	Specimen thickness
$\hat{B}$	Thickness required to have entirely plane stress failure
C_0	Initial specimen compliance
F	Crack geometry function
G	Energy release rate
H	Material deformation function
J	J-integral
J_{el}	Elastic contribution to J-integral

J_{pl}	Plastic contribution to J-integral
$J_{DB,pl.strain}$	J-integral at the ductile to brittle transition in plane strain
J_i^*	J-integral at critical interaction time
$J_{i\ pl.strain}^*$	J-integral at critical interaction time in plane strain
$J_{i\ pl.stress}^*$	J-integral at critical interaction time in plane stress
$J_{i\ BM}^*$	J-integral at critical interaction time in plane stress for blow moulded specimens
$J_{i\ CM}^*$	J-integral at critical interaction time in plane stress for compression moulded specimens
K	Stress intensity factor
L	Specimen length
P	Load
P_i	Initiation load
P_{max}	Maximum load
$S_{i,j}$	Separation parameter
U_i	Mechanical input energy at fracture initiation
U_{el}	Elastic component of the mechanical input energy
$U_{el\ i,BM}$	Elastic component of the mechanical input energy at initiation for blow moulded specimens
$U_{el\ i,CM}$	Elastic component of the mechanical input energy at initiation for compression moulded specimens
U_{pl}	Plastic component of the mechanical input energy
$U_{pl\ i,BM}$	Plastic component of the mechanical input energy at initiation for blow moulded specimens
$U_{pl\ i,CM}$	Plastic component of the mechanical input energy at initiation for compression moulded specimens
W	Specimen width
η_{el}	Elastic *eta* factor
η_{pl}	Plastic *eta* factor
$\phi\left(\dfrac{a}{W}\right)$	Energy release rate calibration factor
σ_Y	Yield stress

1 Introduction

Slow Crack Growth (SCG) is a failure mechanism affecting many thermoplastic polymers when subjected to relatively low stresses. Following load application SCG takes place after a certain incubation time, during which micro-crazes nucleate and grow from pre-existing flaws in the material [1–3]. Once the fibrils connecting the two surfaces of a craze are no longer able to sustain the applied mechanical stress they break, leading to crack initiation and its subsequent propagation. For high stress levels ductile failure occurs before SCG

can develop; for low stresses, the crack slowly propagates with a characteristic "brittle" character, eventually leading to failure in even very long times (years). The resulting fracture surface is usually smooth, with no trace of extensive plastic deformation; multiple cracks, craze remnants and stretched fibrils can be observed as well as alternating bands, corresponding to repeated cycles of craze nucleation and growth and subsequent crack extension [4].

The speed of the phenomena occurring during SCG can significantly increase if the polymer is simultaneously subjected to the mechanical stress and exposed to specific substances, commonly identified as active environments. The generally accepted mechanism at the basis of this acceleration process, called Environmental Stress Cracking (ESC), consists in the diffusion of the active environment within the material, in particular in the crazes; this eventually leads to a local plasticisation and a reduction of the interaction forces between the polymeric macromolecules, thus favouring their mutual disentanglement. As a matter of fact, ESC failures are characterized by reduced crack initiation times and increased crack propagation rates with respect to what occurs in air under the same loading conditions, ultimately decreasing the overall failure time.

The first examples of solvent-induced failures were reported in the literature starting from the '50s; to prevent unexpected breakdown of polymeric components, Environmental Stress Cracking has been extensively studied since. To name several examples, ESC can be observed when exposing polyethylene to aqueous detergents [1,3,5–34] or organic solvents [10,35,36], high impact polystyrene to sunflower oil [11,37–40], polycarbonate to ethanol [41] or fat emulsions [39], phenolic resins to oil [41] or polymethylmethacrylate to different alcohols [8,40,42–44].

Among the various approaches used to analyse these phenomena, those based on fracture mechanics can provide intrinsic polymer properties, which represent a valuable engineering tool. The results obtained from this kind of analysis, in fact, can be used not only for material ranking purposes but also to support mechanical design: they allow to estimate, for example, the expected lifetime of a given component, as reported in [40].

Interestingly, even if many products are characterized by a small thickness and operate under prevailing plane stress conditions, the studies of the ESC resistance of polymers reported in the relevant scientific literature are limited to plane strain conditions. To cover this gap the resistance to SCG and ESC of a blow moulding High-Density Polyethylene (HDPE) grade, used for the manufacturing of bleach bottles, was studied on compression moulded thin specimens subjected to tests under plane stress conditions. The obtained results were then compared with the relevant plane strain behaviour of the same compression moulded polymer, previously studied in [32–34]. Finally, thin specimens, directly obtained from blow moulded bleach bottles, were also tested, thus allowing an investigation of the effect of the material production process on its resistance to SCG and ESC.

2 Experimental

2.1 Materials

A blow moulding HDPE grade having a monomodal molecular weight distribution, previously studied in [32–34] and hereby indicated as HDPE-MONO, was considered. Fracture tests were carried out on specimens cut from compression moulded plates, obtained as described in [33], and from extrusion blow moulded bottles having the geometry shown in Figure 1.
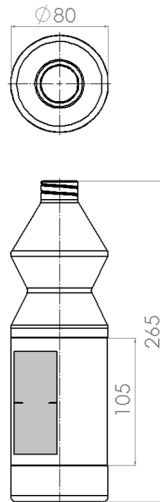
Figure 1 - Geometry of bleach bottles (dimensions in mm). Double Edge Notched Tension (DENT) specimens having a thickness of 0.5 mm were obtained from the central portion of the bottle, with longitudinal orientation parallel to its symmetry axis.

As revealed by Differential Scanning Calorimetry (DSC), the production process influences the final crystallinity of HDPE, its degree equalling 70% and 60% after compression and blow moulding, respectively. Obviously, this difference has an influence on the mechanical properties of the considered material; Figure 2 displays the stress strain curves up to 25% strain obtained at 23°C and 10 mm/min on "type 5" tensile specimens [45]. As expected, the higher degree of crystallinity of the compression moulded material gives rise to higher Young's modulus and yield stress of this specimen.

Further, from Figure 2 it can also be observed that the curves relevant to specimens cut longitudinally and transversally with respect to the blow moulded bottle symmetry axis, are practically coincident; this result indicates that the polymer in the central region of the bottle has similar in-plane orientation along the two directions.
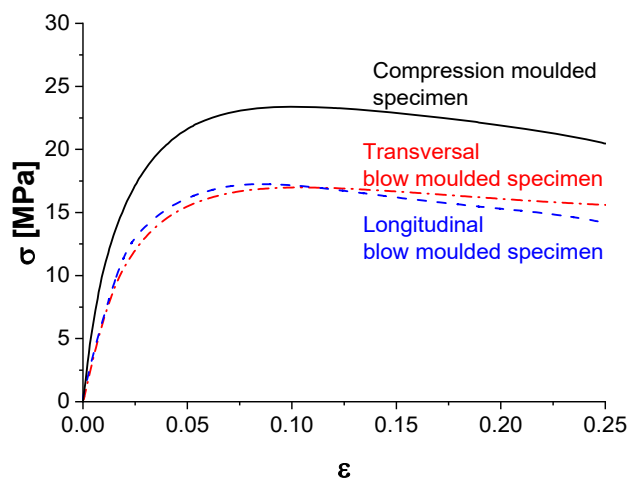

Figure 2 – Initial part of the tensile stress-strain curves obtained at 23°C at 10 mm/min for compression moulded and blow moulded specimens of HDPE-MONO.

To determine the ESC resistance of HDPE-MONO, the employed active environment was derived from a commercial bleach, usually supplied in the bottles considered in this work. This environment was an aqueous solution containing sodium hydroxide, sodium

carbonate, perfume and surfactants (Sol.B in [32–34]); the latter are a well known [1,3,5–34] ESC agent for polyethylene. At variance with commercial detergents, the solution used in the tests did not contain sodium hypochlorite (the actual bleaching agent) since, as proved in [33,34], this chemical does not affect the fracture resistance of the considered HDPE. In such a way the corrosion of metallic mechanical test fixtures was prevented.

2.2   Specimen geometry and test conditions

Double Edge Notched Tension (DENT) specimens having width W of 35 mm and length L 85 mm were die-cut from 1 mm thick compression moulded plates. The manufacturing of plates having a lower thickness was not possible with the equipment used during this work: as revealed from a preliminary production study, 0.5 mm thick plates presented significant distortions and, therefore, they were not adequate for the manufacturing of fracture specimens. A limit for plane stress condition validity was estimated, starting from the stress intensity factor K data reported in [32–34] and from the relevant material yield stress σ_Y; the thickness $\hat{B}$ required to have a plane stress dominated failure, determined from Equation (1) [46], is equal to 6 mm – thus sensibly larger than the actual sample thickness.

$$\hat{B} = \frac{1}{\pi} \cdot \left(\frac{K}{\sigma_Y}\right)^2 \tag{1}$$

Sharp notches with length a of 7 mm, were introduced via die-assisted razor blade sliding, obtaining a final notch tip radius smaller than 5μm. This value is low enough to ensure consistent test results on HDPE and it was the same as that in [33,34], therefore making a direct comparison with the results obtained in those papers possible. Notched specimens were gripped to leave an effective testing size of 35 x 35 mm.

To determine the effect of the degree of crystallinity on SCG and ESC resistance, a second series of specimens, having the same geometry of those just described, was prepared from the 0.5 mm thick central region of the blow moulded bottles, as already shown in Figure 1. Due to the similar in plane orientation of the polymer in this part of the container, all the specimens used for this study were die-cut longitudinally with respect to the symmetry axis, to obtain a higher number of specimens from each bottle. For the blow moulded material, specimens having blunt notches with different lengths and a tip radius of 1 mm, in which the fracture is supposed not to propagate, were also prepared to evaluate the plastic shape factor η_{pl} (see Section 2.3).

Tests were conducted on an Instron 1185R5800 dynamometer and were performed both in air and in the presence of the active environment, already described in Section 2.1 using the environmental chamber developed in [38]. To hasten the fracture phenomenon tests were conducted at 60°C, the maximum temperature above which the solution used separates into water and organic components.

Fracture tests were performed at various constant displacement rates (ranging from 0.0007 mm/min to 500 mm/min). For each displacement rate fracture initiation takes place at a different time, at which fracture toughness was determined as reported in Section 2.3. Fracture toughness vs. crack initiation time curves were then built from this data, both in air and in the presence of the active environment.

Tests conducted in air at a displacement rate higher than 1 mm/min were recorded using a 10 MPixel uEye UI 5490 SE camera with a minimum acquisition rate of 10 fps. For longer tests, photographs were taken using a Nikon D70 photo camera shooting at fixed intervals

ranging from 10 s up to 10 min, depending on the duration of the test. A minimum of 1000 images were acquired for each test.

Due to extensive plastic deformations occurring ahead of the crack tip, a direct determination of crack initiation with sufficient accuracy by visual means had not been possible. Thus, the ligament length was measured from the collected images and plotted as a function of time as shown in Figure 3: in the first part of the curve the ligament length $W - a$ slowly decreased, because of crack tip blunting, then during propagation it did so at a considerably higher rate. Following this observation, a blunting line was extrapolated to the whole duration of the test and the ratio between the actual ligament length data and those extrapolated from the blunting line was evaluated. Crack initiation was assumed to occur when this ratio reached 99%. Although this is an arbitrary threshold, it proved to be an objective and reliable criterion for the determination of the crack initiation time, t_i.
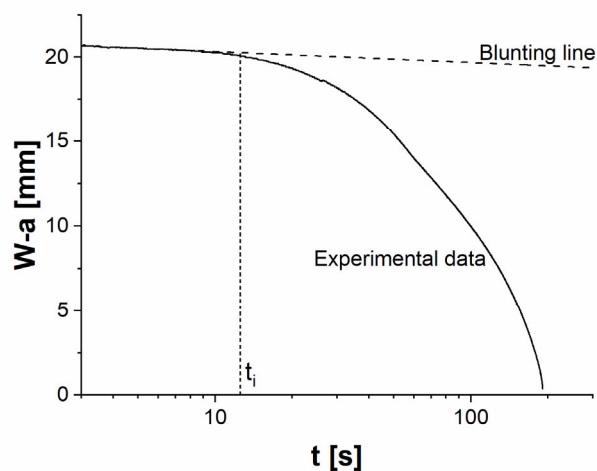
Figure 3 - Ligament length vs. time curve obtained from a test conducted in air. The dotted line represents the crack tip blunting phenomenon; crack initiation was considered to occur at time t_i, corresponding to a 1% difference between the experimental data and the blunting line.

The active environment was a blue-coloured product (see Section 2.1 details about its composition), whose cloudy appearance made *in-situ* visual observation impossible. A transparent solution identical to the blue one, but without the coloured pigment, was sourced from the producer; unfortunately, it was available only in a very scarce amount. With this solution a limited number of tests were conducted, always at the temperature of 60°C, to obtain an alternative initiation criterion, also applicable when using the commercial solution. In particular, considering both the ligament length and load vs. time curves obtained with the transparent solution, it was found that initiation occurred at a load P_i close to the 90% of the maximum load P_{max} for blow moulded specimens and at about the 96% of P_{max} for compression moulded ones. Very similar values of P_i/P_{max} were also found by analysing data from the previous tests performed in air, regardless of the applied displacement rate. Taking advantage of the fact that all the tests were conducted on DENT specimens having an identical geometry, the two identified criteria P_i/P_{max}=90% and P_i/P_{max}=96% were adopted for the determination of fracture initiation of blow moulded and compression moulded specimens, respectively.

The area of the ligament, after the fracture tests, was observed using an Olympus SZ40 stereomicroscope.

2.3 Fracture data analysis

Due to extensive plastic deformations developing ahead of the notch in the thin DENT specimens, a J-integral approach was adopted for the evaluation of fracture data, as opposed to the LEFM-based approach considered in [32–34]. Following the analysis proposed in [47], J-integral can be defined as the sum of an elastic and a plastic contribution:

$$J = J_{el} + J_{pl} = \eta_{el} \frac{U_{el}}{B(W - a)} + \eta_{pl} \frac{U_{pl}}{B(W - a)} \tag{2}$$

in which B is the specimen thickness and $W - a$ is the ligament length, while U_{el} and U_{pl} are the elastic and plastic components of the mechanical input energy. The shape factors η_{el} and η_{pl} depend on the specimen geometry through the ratio of crack length to specimen width; they are called elastic and plastic *eta* factors, respectively. U_{el} and U_{pl} were computed by integrating the area under the two load vs. elastic displacement (P vs. u_{el}) and load vs. plastic displacement (P vs. u_{pl}) curves up to crack initiation.

The elastic displacement u_{el} was calculated as:

$$u_{el} = P \cdot C_0 \tag{3}$$

where C_0 is the initial specimen compliance evaluated from the first part of the load vs. displacement curve, which in the considered case was linear up to a displacement of0.5 mm. The initial compliance was accurately determined for each individual specimen to evaluate u_{el}.

Once u_{el} had been determined, u_{pl} was calculated as

$$u_{pl} = u - u_{el} \tag{4}$$

where u is the overall displacement measured during the test.

For a linear elastic material the J-integral and the energy release rate G are equivalent, therefore η_{el} can be obtained from the energy release rate calibration factor $\phi \left(\frac{a}{W} \right)$ [48]:

$$J_{el} = G = \frac{U_{el}}{BW\phi} = \frac{(W - a)}{W\phi} \cdot \frac{U_{el}}{B(W - a)} = \frac{1 - \frac{a}{W}}{\phi} \cdot \frac{U_{el}}{B(W - a)} = \eta_{el} \cdot \frac{U_{el}}{B(W - a)} \tag{5}$$

$\phi\left(\frac{a}{W}\right)$ was evaluated by computing, via finite element analysis, the compliance of specimens having different crack lengths; η_{el} was then obtained from Equation (5). The energy release rate calibration factor, $\phi\left(\frac{a}{W}\right)$, and the elastic shape factor, η_{el}, for the considered DENT specimen geometry are reported in Figure 4.
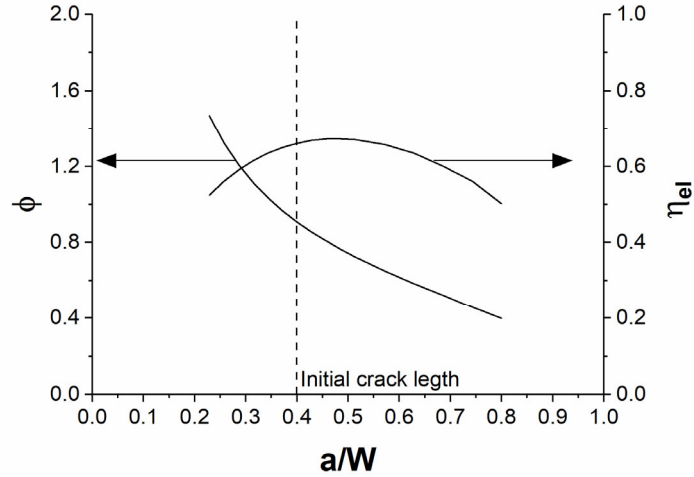

Figure 4 - Energy calibration factor ϕ and elastic shape factor η_{el} for DENT specimens.

The plastic shape factor η_{pl}, instead, was evaluated experimentally using the method based on the load separation criterion also proposed in [47] and applied, more recently, to the characterization of the nonlinear fracture behaviour of polymers [49–58]. According to this theory, for a given material, geometry and loading condition the load P is separable if it can be expressed as the product of a crack geometry function F and of a material deformation function H as per Equation (6):

$$P = F\left(\frac{a}{W}\right) \cdot H\left(\frac{u_{pl}}{W}\right) \tag{6}$$

and if, considering two blunt notched specimens having identical dimensions, with the exception of different notch lengths named a_i and a_j, a separation parameter $S_{i,j}$, constant in the whole domain of the plastic displacement, can be defined as:

$$S_{i,j} = \left.\frac{P(a_i)}{P(a_j)}\right|_{u_{pl}} = \left.\frac{F\left(\frac{a_i}{W}\right) \cdot H\left(\frac{u_{pl}}{W}\right)}{F\left(\frac{a_j}{W}\right) \cdot H\left(\frac{u_{pl}}{W}\right)}\right|_{u_{pl}} = \left.\frac{F\left(\frac{a_i}{W}\right)}{F\left(\frac{a_j}{W}\right)}\right|_{u_{pl}} \tag{7}$$

For a specimen respecting the conditions imposed by Equations (6) and (7), the plastic shape factor η_{pl} can be written as:

$$\eta_{pl} = -\frac{W-a_i}{W} \cdot \frac{dF\left(\frac{a_i}{W}\right)\Big/d\left(\frac{a_i}{W}\right)}{F\left(\frac{a_i}{W}\right)} = \frac{W-a_i}{W} \cdot \frac{dF\left(\frac{W-a_i}{W}\right)\Big/d\left(\frac{W-a_i}{W}\right)}{F\left(\frac{W-a_i}{W}\right)} \tag{8}$$

and can be experimentally determined performing tests on various blunt notched specimens having different ligament lengths. These tests were hence conducted, on DENT specimens, at 60°C and at a constant displacement rate of 10 mm/min. The load vs. plastic displacement curves obtained from these tests, shown in Figure 5, were subsequently used to determine the separation parameter $S_{i,j}$ displayed in Figure 6, in which the specimen with ligament length equal to 23 mm was considered as the reference

one. In the first part of this curve a variable $S_{i,j}$ can be observed and, therefore, the load in the first region of the plastic displacement field is not separable. This is probably related to the fact that, as reported in [59], a separable behaviour can be observed only after the plastic pattern has completely developed; this instance, for the geometry and material considered in this work, seems to occur only after complete ligament yielding. Figure 5 demonstrates how the slope change following the maximum of the curves is reached at different plastic displacements; since $S_{i,j}$ is the ratio of the loads measured at fixed plastic displacement and since the curves becomes all monotonically increasing only after this slope change, a peculiar "fin" shape is present in the $S_{i,j}$ vs. u_{pl} curves of Figure 6. However, after the non separable region a practically constant separation parameter is reached in all the data: these were the values used to evaluate η_{pl}.
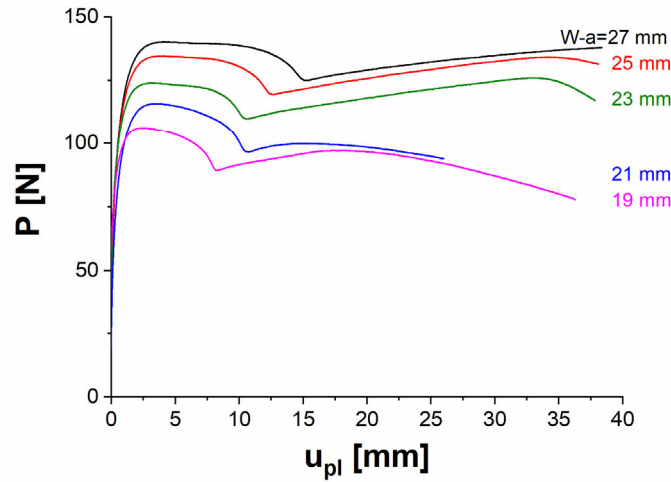
*Figure 5 - Load vs. plastic displacement curves
for blunt notched DENT specimens having different ligament length.*
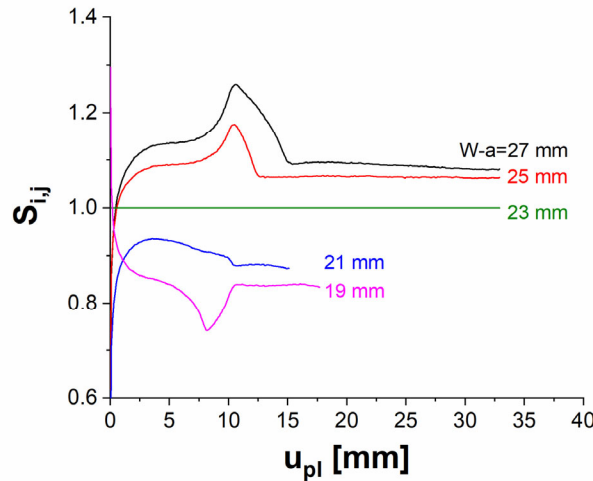
*Figure 6 - Separation parameter vs. plastic displacement curves
for blunt notched DENT specimens having different ligament length.*

The procedure to determine this parameter requires plotting, in a double logarithmic scale, the separation parameter (in the separable region) as a function of $\frac{W-a}{W}$, as done in Figure 7. Data can be fitted using the following expression:

$$S_{i,j} = A \cdot \left(\frac{W - a_i}{W}\right)^m \tag{9}$$

Moreover, since for a fixed reference specimen $F\left(\frac{a_j}{W}\right)$ in Equation (7) is a constant, it can be rewritten as:

$$S_{i,j} = A_1 \cdot F\left(\frac{W - a_i}{W}\right) \tag{10}$$

Combining Equations (9) and (10) the following expression for $F\left(\frac{a_i}{W}\right)$ is obtained:

$$F\left(\frac{W - a_i}{W}\right) = A_2 \cdot \left(\frac{W - a_i}{W}\right)^m \tag{11}$$

Finally, inserting Equation (11) in Equation (8), η_{pl} can be evaluated as:

$$\eta_{pl} = \frac{W - a_i}{W} \cdot \frac{dF\left(\frac{W - a_i}{W}\right) \Big/ d\left(\frac{W - a_i}{W}\right)}{F\left(\frac{W - a_i}{W}\right)} = \frac{W - a_i}{W} \cdot \frac{mA_2 \cdot \left(\frac{W - a_i}{W}\right)^{m-1}}{\left(\frac{W - a_i}{W}\right)^m} = m \tag{12}$$

To determine more accurately the plastic shape factor, $S_{i,j}$ was evaluated multiple times, considering each individual tested specimen as the reference one (Figure 7). The average of the relevant slopes, corresponding to m, was then evaluated as $\eta_{pl} = 0.820 \pm 0.014$.
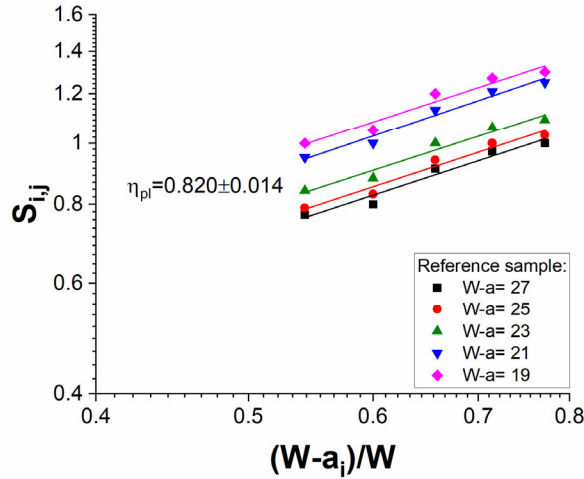
Figure 7 - Separation parameter vs. ligament to width ratio curves.

Once the values of both elastic and plastic shape factors were known, Equation (2) was rewritten as:

$$J = 0.66 \cdot \frac{U_{el}}{B(W - a)} + 0.82 \cdot \frac{U_{pl}}{B(W - a)} \tag{13}$$

finally leading to the evaluation of J-integral at crack initiation, considered as the critical fracture parameter in this study.

3   Results

Figure 8 shows an example of specific load vs. displacement curves obtained from blow moulded specimens tested in air and in the presence of the active environment, performed at the same displacement rate (0.01 mm/min). Even if the two curves are perfectly overlapped up to crack initiation in the active environment (taking place at a displacement of approximately 2.5 mm), the overall behaviour of the two specimens is very different.

Crack initiation in air occurs later. The specific energy U_i/B, evaluated as the area under the curve up to the displacement at crack initiation u_i, decreased by nearly 30% in presence of the active environment. Given this sensitivity, initiation data can be reliably used to characterize the ESC resistance of the considered material. To this purpose, starting from the load displacement curves, and using the procedures described in Section 2, J at crack initiation and the relevant crack initiation time, t_i, were evaluated for each tested specimen; in the following, these two quantities were used to build $\mathrm{Log}(J)$ vs. $\mathrm{Log}(t_i)$ initiation curves.

For a greater clarity, the effect of the stress state and that of the production process are described separately in Section 3.1 and Section 3.2.
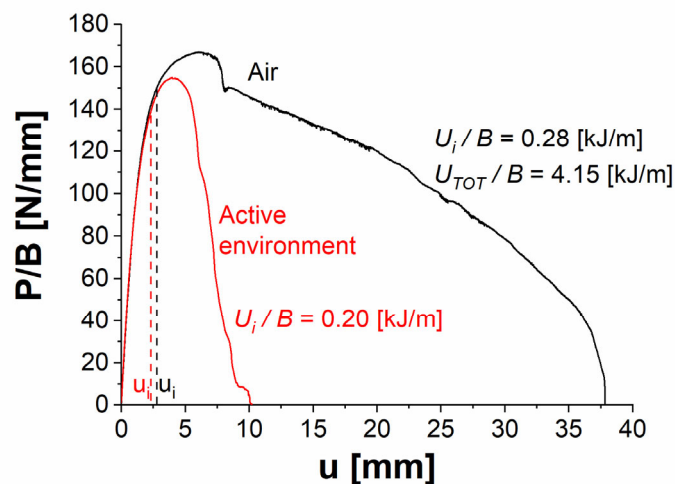
Figure 8 - Specific load vs. displacement curve obtained from blow moulded DENT specimens tested in air and in active environment at a displacement rate of 0.01 mm/min. u_i is the displacement at crack initiation and U_i/B is the specific energy required to have crack initiation.

3.1 Effect of stress state

3.1.1 Fracture behaviour in air

The results obtained from compression moulded specimens tested in air at different displacement rates are shown in Figure 9, where relevant data (black squares) were compared with the known plane strain behaviour (red triangles) of the same material [32–34]. Previous data had been obtained through LEFM and, accordingly, the energy release rate G was taken as an equivalent measure of J.
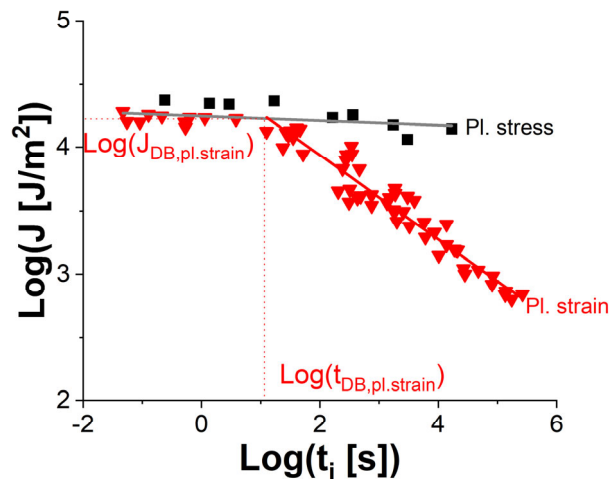
Figure 9 - $Log(J)$ vs. $Log(t_i)$ curves of compression moulded HDPE-MONO tested under plane stress (black squares) and plane strain (red triangles) conditions in air. Plane strain data were reproduced from [32–34].

The variation of the slope of the plane strain curve observed at about 10 s and at a value of J of about 14 kJ/m² corresponds to a ductile to brittle transition, in accordance with findings reported in [60–63] and supported by the fractographic studies conducted in [34].

Plane stress $Log(J)$ vs. $Log(t_i)$ data seem to follow a very similar trend of the curve corresponding to ductile behaviour. Figure 10(a) shows how the broken ligament looks like after a typical test for a plane stress specimen. The overall character of the fracture process seems to be ductile in this case. Within the considered experimental window no slope variation can be detected under plane stress conditions.

(a)

(b)
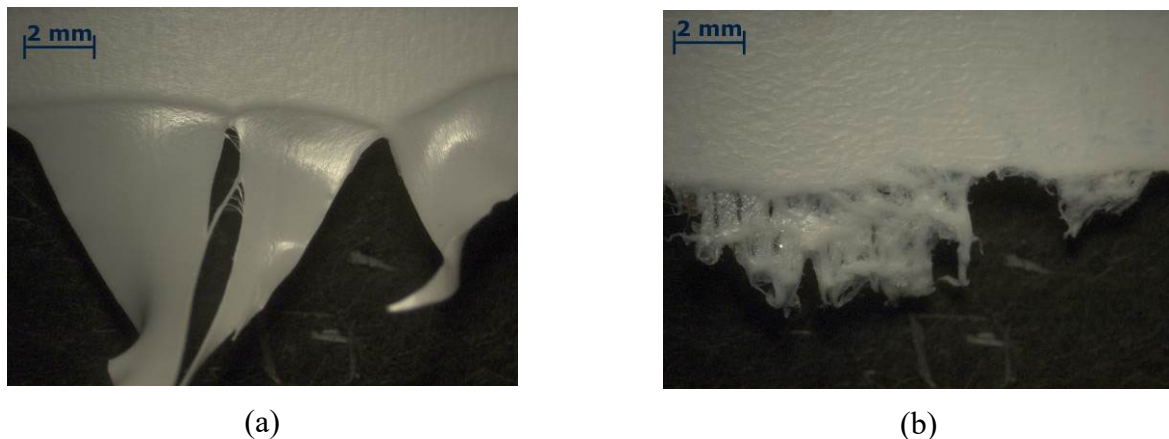
Figure 10 - Examples of the ligaments of two specimens after a fracture test (a) in air and (b) in active environment. The same fracture phenomenology was observed for compression moulded and blow moulded specimens.

3.1.2 Fracture behaviour in active environment

Figure 11 reports fracture data showing the effect of the environment for both stress states in comparison with the relevant behaviour in air; for the latter case data points were replaced with the trend lines depicted in Figure 9, to avoid excessive clutter in the graph.
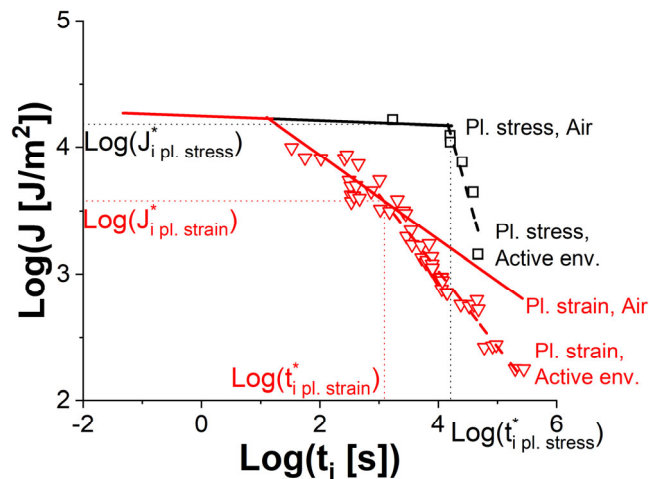
Figure 11 - $Log(J)$ vs. $Log(t_i)$ data for compression moulded HDPE-MONO tested under plane stress and plane strain conditions in air (continuous line) and in active environment (symbols and dashed lines). Plane strain data were reproduced from [32–34].

Similarly to what had been observed in [38,40,44], the active environment causes a sharp reduction in the fracture resistance only after a critical interaction time t_i^*, which can be identified by looking at the intersection of the air and environment branches of the $Log(J)$ vs. $Log(t_i)$ curve. Under plane strain conditions this intersection occurs when the fracture mechanism in air is already brittle failure, which is governed by crazing. Under plane stress crazing does not occur or its occurring is very limited, and interestingly the environment itself is causing a ductile to brittle transition: a pronounced slope change in the $Log(J)$ vs. $Log(t_i)$ curve can be identified and the appearance of specimen ligaments after the tests (see Figure 10(b)) is indeed completely different. A direct consequence of this difference, related to the prevalent stress state, can be observed by comparing the two t_i^* values corresponding to the two critical J-integral values, J_i^*: since under plane strain conditions the diffusion of the active environment in the craze ahead of the crack tip is easier, due to the high surface to volume ratio in this region, $t_{i\ pl.strain}^*$ is shorter than $t_{i\ pl.stress}^*$.

3.2 Effect of processing

3.2.1 Fracture Behaviour in air

Figure 12 displays the comparison between the $Log(J)$ vs. $Log(t_i)$ curves of compression moulded (CM, already shown in Figure 9) and blow moulded (BM) HDPE, both tested under plane stress conditions. The two curves have a similar slope and in both cases a ductile failure was observed. As expected, due to the higher degree of crystallinity of compression moulded specimens, their relevant fracture toughness J is higher.
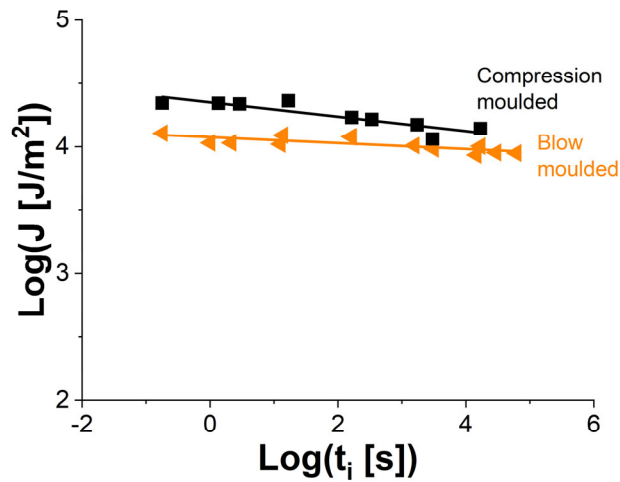
Figure 12 - $Log(J)$ vs. $Log(t_i)$ curves of blow moulded and compression moulded HDPE-MONO tested in air under plane stress conditions.

To clarify the phenomena involved during the fracture process, elastic (J_{el}) and plastic (J_{pl}) contributions to J were separately analysed. An example of the raw data processing is reported in Figure 13.

In Figure 14 two components of J are plotted as a function of the crack initiation time. Both J_{el} and J_{pl} show a dependence on the initiation time, thus suggesting that the variation of J with the initiation time is related to the time dependence of both elastic and plastic components. The elastic component J_{el} (Figure 14a) seems to be unaffected by the production process while a relatively higher value of J_{pl} (Figure 14b) can be observed for compression moulded specimens. In both cases the plastic contribution to J is predominant with respect to the elastic one.
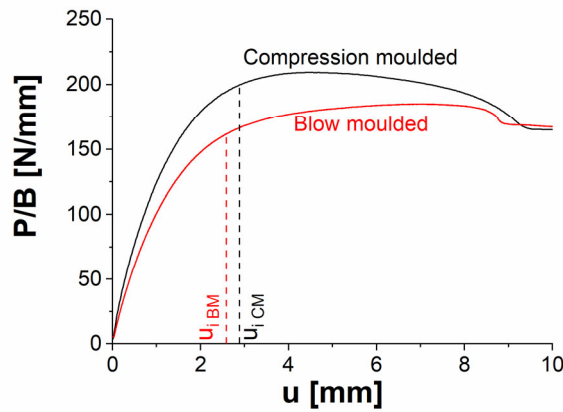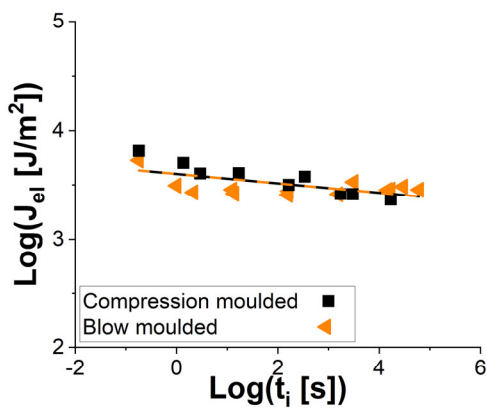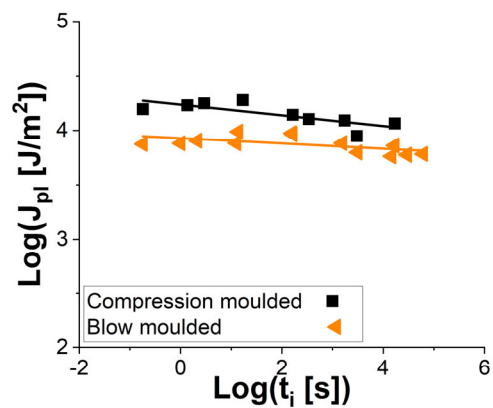
(a)
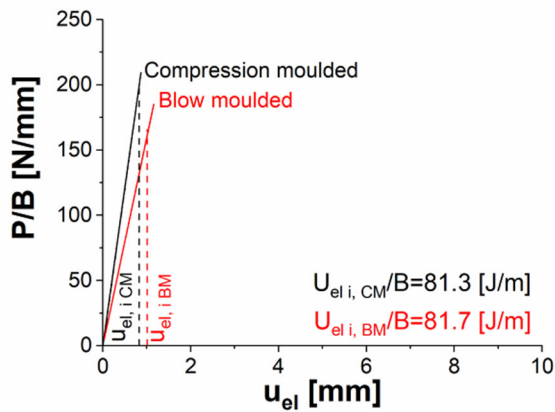
(b)
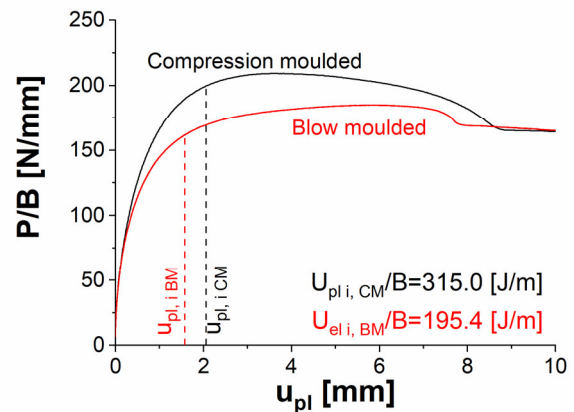
(c)

Figure 13 –Specific load vs. (a) displacement (b) elastic displacement (c) plastic displacement for compression moulded and blow moulded HDPE-MONO tested in air under plane stress conditions at a displacement rate of 0.1 mm/min. Consistent results were obtained from tests at different displacement rates.

(a)

(b)

Figure 14 - (a) elastic and (b) plastic contributions to J-integral of specimens tested in air under plane stress conditions.

3.2.2 Fracture behaviour in active environment

Fracture toughness data measured in presence of the active environment is plotted in Figure 15. Despite the different behaviour in air, which is reflected on the slightly higher value of $J_{i\ CM}^{*}$ in comparison to $J_{i\ BM}^{*}$, the critical interaction time t_{i}^{*} is practically the same

for compression moulded and blow moulded specimens. Beyond t_i^*, in presence of the active environment, data from compression moulded and blow moulded specimens do not exhibit significant differences.
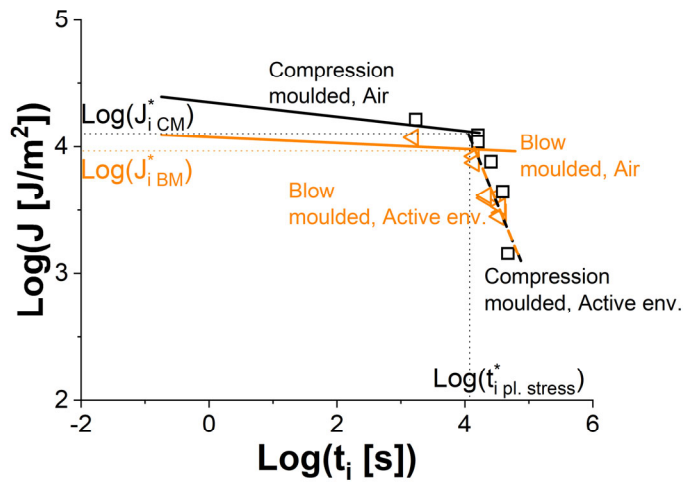

Figure 15 - $Log(J)$ vs. $Log(t_i)$ curves of blow moulded and compression moulded HDPE-MONO tested in air (continuous lines) and in active environment (symbols) under plane stress conditions.

Analysing separately the two contributions to J, as done in Figure 16, both J_{el} and J_{pl} strongly decrease with increasing t_i, for initiation times greater than the critical interaction time t_i^*. In both cases, data from compression moulded and blow moulded specimens seem to lie on the same curve. Figure 17 reports for all specimens tested the ratio between the J_{el} and J_{pl} values obtained in air and in active environment. It can be observed that the decrease due to the presence of the active environment is larger for J_{pl} than for J_{el} thus suggesting that the environment causes mainly a reduction of the plastic deformations before crack initiation. These findings are consistent with the observation of the micrographs in Figure 10, showing the evident decrease of plasticity in the compression moulded specimen tested in the active environment compared to the one tested in air.
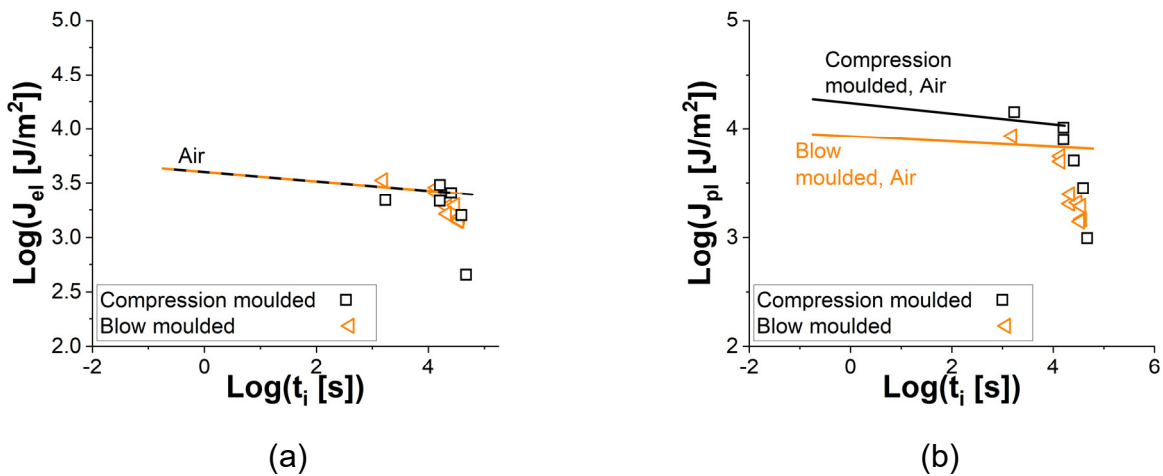

(a)   (b)

Figure 16 - (a) elastic and (b) plastic contributions to J of specimens tested in air (continuous line) and in environment (symbols).
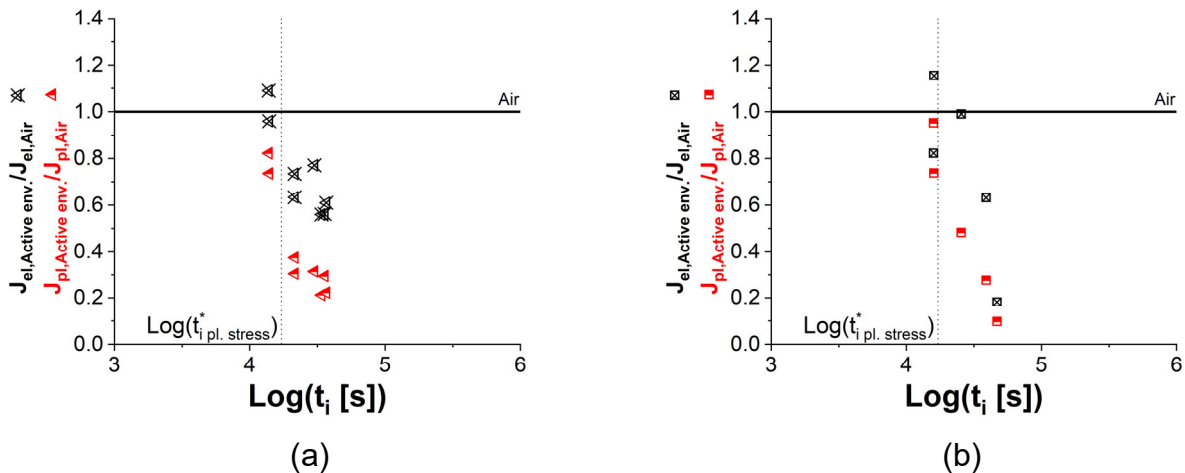
Figure 17 – Variation of the elastic and plastic contributions to J due to the presence of the active environment in (a) compression moulded and (b) blow moulded specimens.

4 Discussion

As described in [36,61,64], when a semicrystalline polymer like HDPE is mechanically loaded, the more compliant amorphous phase, mainly constituted by tie molecules connecting adjacent crystallites, will deform easily at first. However, if the mechanical stress is sufficiently high, once the tie molecules reach their full extension irreversible shear deformations take place in the crystalline phase causing a fragmentation of polymer crystals into smaller units called "mosaic blocks" and leading to a ductile failure. On the other hand, if the mechanical stress is not sufficient to plastically deform polymer crystallites, tie molecules disentanglement takes place instead and brittle failure usually occurs. The results obtained in the present work are in good agreement with this deformation model, with the identification of the different active mechanisms depending on the applied loading conditions.

Considering first the behaviour in air, it was observed in Figure 9 that all the plane stress data follow a trend very similar to the curve that under plane strain conditions corresponds to a ductile fracture. Since ductile fracture mainly takes place in the crystalline phase it is reasonable to expect that the same amount of specific energy will be required to drive an increase in the crack length for the two stress states. Conversely, if the degree of crystallinity is significantly different, as is the case for the blow moulded and compression moulded specimens, a higher amount of energy will be associated to crack extension of the more crystalline material, as revealed by the comparison of J and, in particular, of J_{pl} (see Figure 12 and Figure 14, respectively). When fracture occurs for a value of J below 14 kJ/m², a brittle failure mechanism becomes predominant under plane strain conditions, indicating that in this regime the fracture process is governed by tie molecule disentanglement. For specimens under plane stress no evidence of a brittle regime was found in air within the explored time range.

Regarding the effect of the active environment, for times longer than t_i^*, a local plasticization of the material is likely to occur at the crack tip, where crazes nucleate [18,36,65]; the consequent acceleration of tie molecules disentanglement therefore promotes brittle failure. For the material studied in this work, under plane strain conditions this plasticization begins to occur when crazing is already the dominant (brittle) fracture mechanism; conversely, under plane stress conditions at the relevant critical interaction time it is the environment itself which causes a ductile to brittle transition. It is interesting to

compare the critical interaction times t_i^* obtained for the two stress states: under plane stress conditions (under which shear yielding is mainly occurring) a longer time is required by the active environment to significantly interact with the tie molecules in the amorphous phase. Obviously, due to the different failure mode observed in air for the two stress states, the relevant $J_{pl.stress}^*$ is higher than $J_{pl.strain}^*$.

The production process is not expected to modify the aspects of the molecular structure which control ESC resistance, such as the molecular weight distribution [2,66] or the presence of side groups in the polymeric chain [67,68]; in turn, as expected, the compression moulding and blow moulding specimens significantly differed in their degrees of crystallinity. Accordingly, (i) the level of J is different in air under plane stress conditions, where ductile fracture takes place and the behaviour of the crystalline phase dominates failure; (ii) in the presence of the active environment, where the failure mode switches to tie molecules-controlled brittle fracture, there is no apparent effect of the production process and all the relevant data lie on the same curve, as observed in Figure 15.

5   Conclusions

The Slow Crack Growth and Environmental Stress Cracking of a high density polyethylene were investigated under plane stress conditions following a *J*-integral approach. The main findings of this research are:

- The ductile to brittle transition previously observed under plane strain tests in air on the same polyethylene was not observed under plane stress. In this case only ductile failure occurred. Nevertheless, the ductile fracture part of *J* vs. fracture initiation time curves is the same irrespective of the applied stress state, indicating that the same mechanism, likely related to the fragmentation of polymer crystalline domains, controls failure.

- The critical interaction time necessary for the active environment to cause Environmental Stress Cracking was an order of magnitude longer under plane stress. This can be explained considering the different active failure mechanisms. Under plane strain brittle failure is already dominant when the environment begins to play a role: when a crack propagates starting from a craze, the environment likely accelerates the process of tie molecule disentanglement. Under plane stress instead, ductile fracture with extensive shear yielding occurs over the whole range of initiation times explored and the penetration of the solution into the amorphous phase is hindered. A much longer time is thus required to grant sufficient penetration and finally activate tie molecules disentanglement, so that brittle fracture can take place.

- Tests under plane stress on specimens with two different degrees of crystallinity, as obtained by two different production processes, showed that a higher value of this variable gives rise to increased fracture toughness in air. In presence of the active environment the behaviour of the two specimens was instead very similar and the obtained data lie on the same *J* vs. fracture initiation time curve. The analysis of the individual elastic and plastic components of *J* suggests that plastic deformations of polyethylene crystalline domains are suppressed in presence of the active environment, with tie molecule disentanglement likely becoming the dominant failure mechanism.

These findings highlight the complex interrelation existing between ESC and the applied stress state. Given the high number of applications in which ESC limits product lifetime, it is of great importance that future studies do not neglect these aspects by limiting themselves to typical plane strain analysis. At the same time, a better understanding of the specific role played by the production process in determining environmental fracture

resistance will hopefully provide material producers with useful insight to develop better solutions.

6 Acknowledgements

7 References

[1]   Lustiger A, Corneliussen RD. The role of crazes in the crack growth of polyethylene. J Mater Sci 1987;22:2470–6. https://doi.org/10.1007/BF01082132.

[2]   Huang Y-L, Brown N. The effect of molecular weight on slow crack growth in linear polyethylene homopolymers. J Mater Sci 1988;23:3648–55. https://doi.org/10.1007/BF00540508.

[3]   Men YF, Rieger J, Enderle HF, Lilge D. The mobility of the amorphous phase in polyethylene as a determining factor for slow crack growth. Eur Phys J E 2004;15:421–5. https://doi.org/10.1140/epje/i2004-10059-3.

[4]   Jansen JA. Environmental Stress Cracking – THE PLASTIC KILLER. Adv Mater Process 2004;162:50–3.

[5]   Chan MK V, Williams JG. Slow stable crack growth in high density polyethylenes. Polymer 1983;24:234–44. https://doi.org/10.1016/0032-3861(83)90139-8.

[6]   Tonyali K, Brown HR. Effects of detergent concentration and ethylene oxide chain length of the detergent molecule on stress-cracking of low-density polyethylene. J Mater Sci 1987;22:3287–92. https://doi.org/10.1007/BF01161193.

[7]   Rink M, Frassine R, Mariani P, Carianni G. Effects of detergent on crack initiation and propagation in polyethylenes. Eur Struct Integr Soc 2003;32:103–14. https://doi.org/10.1016/S1566-1369(03)80087-0.

[8]   Williams JG, Marshall GP. Environmental Crack and Craze Growth Phenomena in Polymers. Proc R Soc Lond A Math Phys Sci 1975;342:55–77. https://doi.org/http://doi.org/10.1098/rspa.1975.0012.

[9]   Tonyali K, Brown HR. On the applicability of linear elastic fracture mechanics to environmental stress cracking of low-density polyethylene. J Mater Sci 1986;21:3116–24. https://doi.org/10.1007/BF00553345.

[10]   Tonyali K, Rogers CE, Brown HR. Stress-cracking of polyethylene in organic liquids. Polymer 1987;28:1472–7. https://doi.org/10.1016/0032-3861(87)90344-2.

[11]   Kamaludin MA, Patel Y, Blackman BRK, Williams JG. Fracture mechanics testing for environmental stress cracking in thermoplastics. Procedia Struct Integr 2016;2:227–34. https://doi.org/10.1016/j.prostr.2016.06.030.

[12] Cheng JJ, Polak MA, Penlidis A. Influence of micromolecular structure on environmental stress cracking resistance of high density polyethylene. Tunn Undergr Sp Technol 2011;26:582–93. https://doi.org/10.1016/j.tust.2011.02.003.

[13] Lustiger A, Markham RL, Epstein MM. Environmental stress crack growth in medium-density polyethylene pipe. J Appl Polym Sci 1981;26:1049–56. https://doi.org/10.1002/app.1981.070260327.

[14] Belcher JL, Brown HR. Crack branching and arrest in environmental cracking of polyethylene. J Mate 1986;21:717–24. https://doi.org/10.1007/BF01145546.

[15] Chang P, Donovan JA. Crack size independence of the crack driving force in the buckled plate specimen. J Mater Sci 1989;24:816–20. https://doi.org/10.1007/BF01148762.

[16] Ward AL, Lu X, Huang Y, Brown N. The mechanism of slow crack growth in polyethylene by an environmental stress cracking agent. Polymer 1991;32:2172–8. https://doi.org/10.1016/0032-3861(91)90043-I.

[17] Lu X, Zhou Z, Brown N. A Sensitive Mechanical Test for Slow Crack Growth in Polyethylene. Polym Eng Sci 1997;37:1896–900. https://doi.org/10.1002/pen.11839.

[18] Fleissner M. Experience With a Full Notch Creep Test in Determining the Stress Crack Performance of Polyethylenes. Polym Eng Sci 1998;38:330–40. https://doi.org/10.1002/pen.10194.

[19] Plummer CJ., Goldberg A, Ghanem A. Micromechanisms of slow crack growth in polyethylene under constant tensile loading. Polymer 2001;42:9551–64. https://doi.org/10.1016/S0032-3861(01)00476-1.

[20] Ayyer R, Hiltner A, Baer E. A fatigue-to-creep correlation in air for application to environmental stress cracking of polyethylene. J Mater Sci 2007;42:7004–15. https://doi.org/10.1007/s10853-006-1108-2.

[21] Pinter G, Haager M, Lang RW. Influence of nonylphenol-polyglycol-ether environments on the results of the full notch creep test. Polym Test 2007;26:700–10. https://doi.org/10.1016/j.polymertesting.2007.01.010.

[22] Ayyer R, Hiltner A, Baer E. Effect of an environmental stress cracking agent on the mechanism of fatigue and creep in polyethylene. J Mater Sci 2008;43:6238–53. https://doi.org/10.1007/s10853-008-2926-1.

[23] Choi B-H, Weinhold J, Reuschle D, Kapu M. Modeling of the Fracture Mechanism of HDPE Subjected to Environmental Stress Crack Resistance Test. Polym Eng Sci 2009;49:2085–91. https://doi.org/10.1002/pen.21458.

[24] Schilling M, Niebergall U, Böhning M. Full notch creep test (FNCT) of PE-HD – Characterization and differentiation of brittle and ductile fracture behavior during environmental stress cracking (ESC). Polym Test 2017;64:156–66. https://doi.org/10.1016/j.polymertesting.2017.09.043.

[25] Andena L, Castellani L, Castiglioni A, Mendogni A, Rink M, Sacchetti F, et al. Environmental crack initiation and propagation in polyethylene under different loading conditions. Proc. 15th Int. Conf. Deform. Yield Fract. Polym., 2012, p. 182–5.

[26] A. Sharif, N. Mohammadi SRG. Model Prediction of the ESCR of Semicrystalline Polyethylene: Effects of Melt Cooling Rate. J Appl Polym Sci 2009;112:3249–56. https://doi.org/10.1002/app.29893.

[27] Lagarón JM, Pastor JM, Kip BJ. Role of an active environment of use in an environmental stress crack resistance (ESCR) test in stretched polyethylene: A vibrational spectroscopy and a SEM study. Polymer 1999;40:1629–36. https://doi.org/10.1016/S0032-3861(98)00406-6.

[28] Lagarón JM, Capaccio G, Rose LJ, Kip BJ. Craze morphology and molecular orientation in the slow crack growth failure of polyethylene. J Appl Polym Sci 2000;77:283–96. https://doi.org/10.1002/(SICI)1097-4628(20000711)77:2<283::AID-APP5>3.0.CO;2-0.

[29] Kurelec L, Teeuwen M, Schoffeleers H, Deblieck R. Strain hardening modulus as a measure of environmental stress crack resistance of high density polyethylene. Polymer 2005;46:6369–79. https://doi.org/10.1016/j.polymer.2005.05.061.

[30] Munaro M, Akcelrud L. Polyethylene blends: A correlation study between morphology and environmental resistance. Polym Degrad Stab 2008;93:43–9. https://doi.org/10.1016/j.polymdegradstab.2007.10.017.

[31] Cazenave J, Sixou B, Seguela R. Structural Approaches of Polyethylene Environmental Stress-Crack Resistance. Oil Gas Sci Technol 2006;61:735–42. https://doi.org/10.2516/ogst:2006011.

[32] Contino M, Andena L, La Valle V, Rink M, Marra G, Resta S. A comparison between K and G approaches for a viscoelastic material: the case of environmental stress cracking of HDPE. Mech Time-Dependent Mater 2020;24:381–94. https://doi.org/10.1007/s11043-019-09426-z.

[33] Contino M, Andena L, Rink M, Marra G, Resta S. Time-temperature equivalence in environmental stress cracking of high-density polyethylene. Eng Fract Mech 2018;203:32–43. https://doi.org/10.1016/j.engfracmech.2018.04.034.

[34] Contino M, Andena L, Rink M, Colombo A, Marra G. Fracture of high-density polyethylene used for bleach bottles. Procedia Struct Integr 2016;2:213–20. https://doi.org/10.1016/j.prostr.2016.06.028.

[35] Schoeffl PF, Bradler PR, Lang RW. Yielding and crack growth testing of polymers under severe liquid media conditions. Polym Test 2014;40:225–33. https://doi.org/10.1016/j.polymertesting.2014.09.005.

[36] Yarysheva AY, Rukhlya EG, Yarysheva LM, Bagrov D V., Volynskii AL, Bakeev NF. The structural evolution of high-density polyethylene during crazing in liquid medium. Eur Polym J 2015;66:458–69. https://doi.org/10.1016/j.eurpolymj.2015.03.003.

[37] Andena L, Rink M, Marano C, Briatico-Vangosa F, Castellani L. Effect of processing on the environmental stress cracking resistance of high-impact polystyrene. Polym Test 2016;54:40–7. https://doi.org/10.1016/j.polymertesting.2016.06.017.

[38] Andena L, Castellani L, Castiglioni A, Mendogni A, Rink M, Sacchetti F. Determination of environmental stress cracking resistance of polymers: Effects of loading history and testing configuration. Eng Fract Mech 2013;101:33–46. https://doi.org/10.1016/j.engfracmech.2012.09.004.

[39] Altstaedt V, Keiter S, Renner M, Schlarb A. Environmental stress cracking of polymers monitored by fatigue crack growth experiments. Macromol Symp 2004;214:31–46. https://doi.org/10.1002/masy.200451004.

[40] Kamaludin MA, Patel Y, Williams JG, Blackman BRK. A fracture mechanics approach to characterising the environmental stress cracking behaviour of thermoplastics. Theor Appl Fract Mech 2017;92:373–80. https://doi.org/10.1016/j.tafmec.2017.06.005.

[41] Arnold JC. The influence of liquid uptake on environmental stress cracking of glassy polymers. Mater Sci Eng A 1995;197:119–24. https://doi.org/10.1016/0921-5093(94)09759-3.

[42] Arnold JC. The effects of diffusion on environmental stress crack initiation in PMMA. J Mater Sci 1998;33:5193–204. https://doi.org/10.1023/A:1004431920449.

[43] Higuchi Y. Observation of Environmental Stress Cracking in Polymethylmethacrylate by Using the Chemiluminescence Method. Mater Sci Appl 2015;6:1084–8. https://doi.org/10.4236/msa.2015.611107.

[44] Ng SK, Kamaludin MA, Dear JP, Blackman BR. Environmental effects in biaxially orientated Polymethyl Methacrylate. Procedia Struct Integr 2018;13:304–10. https://doi.org/10.1016/j.prostr.2018.12.051.

[45] EN ISO 527-3: Plastics - Determination of tensile properties - Part 3: Test conditions for films and sheets 1995.

[46] Williams JG. Fracture mechanics of polymers. Chichester: Limited, Ellis Horwood; 1984.

[47] Sharobeam MH, Landes JD. The load separation criterion and methodology in ductile fracture mechanics. Int J Fract 1991;47:81–104. https://doi.org/10.1007/BF00032571.

[48] ISO 13586: Plastic - Determination of the fracture toughness (GIC and KIC) - Linear elastic fracture mechanics (LEFM) approach 2003.

[49] Bernal, C.R.; Montemartini, P.E.; Frontini PM. The Use of Load Separation Criterion and Normalization Method in Ductile Fracture Characterization of Thermoplastic Polymers. J Polym Sci 1996;34:1869–80. https://doi.org/10.1002/(SICI)1099-0488(199608)34:11<1869::AID-POLB4>3.0.CO;2-N.

[50] Bernal C, Cassanelli A, Frontini P. On the applicability of the load separation criterion to acrylonitrile/butadiene/styrene terpolymer resins. Polymer 1996;37:4033–9. https://doi.org/10.1016/0032-3861(96)00232-7.

[51] Wainstein J, Frontini PM, Cassanelli AN. J-R curve determination using the load separation parameter Spb method for ductile polymers. Polym Test 2004;23:591–8. https://doi.org/10.1016/j.polymertesting.2003.10.010.

[52] Baldi F, Riccò T. High-rate J-testing of toughened polyamide 6/6: Applicability of the load separation criterion and the normalization method. Eng Fract Mech 2005;72:2218–31. https://doi.org/10.1016/j.engfracmech.2005.02.002.

[53] Baldi F, Agnelli S, Riccò T. On the applicability of the load separation criterion in determining the fracture resistance (JIc) of ductile polymers at low and high loading rates. Int J Fract 2010;165:105–19. https://doi.org/10.1007/s10704-010-9510-9.

[54] Frontini PM, Fasce LA, Rueda F. Non linear fracture mechanics of polymers: Load Separation and Normalization methods. Eng Fract Mech 2012;79:389–414. https://doi.org/10.1016/j.engfracmech.2011.11.020.

[55] Baldi F, Agnelli S, Riccò T. On the determination of the point of fracture initiation by the load separation criterion in J-testing of ductile polymers. Polym Test 2013;32:1326–33. https://doi.org/10.1016/j.polymertesting.2013.08.007.

[56] Agnelli S, Baldi F, Blackman BRK, Castellani L, Frontini PM, Laiarinandrasana L, et al. Application of the load separation criterion in J-testing of ductile polymers: A round-robin testing exercise. Polym Test 2015;44:72–81. https://doi.org/10.1016/j.polymertesting.2015.03.019.

[57] Agnelli S, Baldi F, Castellani L, Pisoni K, Vighi M, Laiarinandrasana L. Study of the plastic deformation behaviour of ductile polymers: Use of the material key curves. Mech Mater 2018;117:105–15. https://doi.org/10.1016/j.mechmat.2017.11.002.

[58] Baldi F, Agnelli S, Andena L, Blackman B, Castellani L, Frontini P, et al. Determination of the Fracture Resistance of Ductile Polymers: The ESIS TC4 Recent Experience. Mater Perform Charact 2020. https://doi.org/10.1520/MPC20190175.

[59] Sharobeam MH, Landes JD. The load separation and ηpl development in precracked specimen test recordsdevelopment in precracked specimen test records. Int J Fract 1993;59:213–26. https://doi.org/10.1007/BF02555184.

[60] Andena L, Rink M, Frassine R, Corrieri R. A fracture mechanics approach for the prediction of the failure time of polybutene pipes. Eng Fract Mech 2009;76:2666–77. https://doi.org/10.1016/j.engfracmech.2009.10.002.

[61] Lustiger A. Environmental Stress Cracking: The Phenomenon and Its Utility. In: Brostow W, Corneliussen RD, editors. Fail. Plast., Munich, Vienna, New York: Hanser Publishers; 1986, p. 305–29.

[62] Krishnaswamy RK. Analysis of ductile and brittle failures from creep rupture testing of high-density polyethylene (HDPE) pipes. Polymer 2005;46:11664–72. https://doi.org/10.1016/j.polymer.2005.09.084.

[63] Deblieck RAC, Van Beek DJM, Remerie K, Ward IM. Failure mechanisms in polyolefines: The role of crazing, shear yielding and the entanglement network. Polymer 2011;52:2979–90. https://doi.org/10.1016/j.polymer.2011.03.055.

[64] Lustiger A, Markham RL. Importance of tie molecules in preventing polyethylene fracture under long-term loading conditions. Polymer 1983;24:1647–54. https://doi.org/10.1016/0032-3861(83)90187-8.

[65] Kurelec L, Teeuwen M, Schoffeleers H, Deblieck R. Strain hardening modulus as a measure of environmental stress crack resistance of high density polyethylene. Polymer 2005;46:6369–79. https://doi.org/10.1016/j.polymer.2005.05.061.

[66] Brown N, Ward IM. The influence of morphology and molecular weight on ductile-brittle transitions in linear polyethylene. J Mater Sci 1983;18:1405–20. https://doi.org/10.1007/BF01111960.

[67] Brown N, Lu X, Huang Y, Harrison IP, Ishikawa N. The fundamental material parameters that govern slow crack growth in linear polyethylenes. Plast Rubber Compos Process Appl 1992;17:255–8.

[68] Huang Y, Brown N. The dependence of butyl branch density on slow crack growth in polyethylene: kinetics. J Polym Sci Part B Polym Phys 1990;28:2007–21. https://doi.org/10.1002/polb.1990.090281110.